HHS Public Access

Author manuscript

Nat Struct Mol Biol. Author manuscript; available in PMC 2017 January 20.

Published in final edited form as:

Nat Struct Mol Biol. 2016 August ; 23(8): 744–751. doi:10.1038/nsmb.3262.

Lipids modulate the conformational dynamics of a secondary multidrug transporter

Chloé Martens[1], **Richard A Stein**[2], **Matthieu Masureel**[1], **Aurélie Roth**[1], **Smriti Mishra**[2], **Rosie Dawaliby**[1], **Albert Konijnenberg**[3], **Frank Sobott**[3], **Cédric Govaerts**[1,4], and **Hassane S Mchaourab**[2,4]

[1]Department of Chemistry, Center for Structural Biology and Bioinformatics, Université Libre de Bruxelles, Brussels, Belgium

[2]Department of Molecular Physiology and Biophysics, Vanderbilt University Medical Center, Nashville, TN, USA

[3]Department of Chemistry, University of Antwerp, Antwerp, Belgium

Abstract

Direct interactions with lipids have emerged as key determinants of the folding, structure and function of membrane proteins, but an understanding of how lipids modulate protein dynamics is still lacking. Here, we systematically explored the effects of lipids on the conformational dynamics of the proton-powered, multidrug transporter LmrP from *Lactococcus lactis* utilizing the pattern of distances between spin label pairs previously shown to fingerprint alternating access of the protein. We uncover at the molecular level how the lipid headgroups shape the conformational energy landscape of the transporter. The model emerging from our data hypothesizes a direct interaction between lipid headgroups and a conserved motif of charged residues that control the conformational equilibrium through an interplay of electrostatic interactions within the protein. Together, our data lay the foundation for a comprehensive model of secondary multidrug transport in lipid bilayers.

There is overwhelming consensus that the biological membrane must play a critical role in membrane protein structure, stability and function owing to its unique physicochemical properties such as dielectric constant, lateral pressure, curvature and thickness [1–6]. It has long been recognized that lipid molecules directly interact with membrane proteins with high affinity [7–9]. Earlier work highlighted that phospholipids and sterols can modulate structure and function of ion channels [10,11], and a flurry of recent studies have demonstrated

Correspondence should be addressed to C.G. (cedric.govaerts@ulb.ac.be) and H.M. (hassane.mchaourab@vanderbilt.edu).
[4]These authors are co-last authors

Author Contributions

C.M., H.M. and C.G.: experimental design. M.M, S.M. A.R and C.M: mutagenesis, expression, activity, purification, reconstitution and labeling experiments. R.S: EPR measurements. R.S, C.M and H.M.: DEER data analysis. C.G. and C.M.: molecular modeling. C.M and A.R: transport assays. A.K. and F.S.: native MS measurements and data analysis. R.D: LC-MS/MS measurements and analysis. C.G. and H.M. oversaw all aspects of the experiments and manuscript preparation. All authors participated in interpreting the data and writing the paper.

Competing Financial Interests Statement

The authors declare no competing financial interests.

that bound lipids can affect folding, impart stability and modulate the function and physiological role of membrane proteins [12–17]. For example, lipids act as allosteric modulators of the β2 adrenergic receptor activation by its cognate ligands [18]. In dopamine-mediated neurotransmission, the lipid PIP_2 controls signaling events associated with physiological and behavioral consequences [19] and computational models have hypothesized interactions of PIP_2 with specific structural elements of neurotransmitter transporters [20,21]. Because most membrane proteins undergo transitions between distinct conformations, the lipid modulation of their function must be underpinned by direct effects on the underlying dynamics [22]. However, how the lipid bilayer impacts the structural dynamics of embedded proteins remains poorly understood.

We set out to investigate in detail how lipids shape the conformational energy landscape of a membrane protein, the multidrug transporter LmrP from *Lactococcus lactis*. LmrP, a member of the Major Facilitator Superfamily (MFS), couples the downhill translocation of protons along their transmembrane gradient to the uphill transport of hydrophobic cytotoxic compounds [23,24]. Unlike substrate-specific MFS transporters, multidrug antiporters have evolved to be polyspecific and to potentially bind their substrates from the inner leaflet of the bilayer [25,26]. Their ability to bind structurally and chemically dissimilar substrates challenges the notions of high-affinity substrate binding and strict ion-substrate coupling [27–29]. Furthermore, the active efflux of diverse cytotoxic compounds through secondary multidrug transporters contributes to bacterial antibiotic resistance [26,30,31]. In this context, an accurate description of the mechanism of these transporters in a native-like environment would be valuable from a fundamental as well as a clinical standpoint.

We recently described the proton- and substrate-dependent alternating access of LmrP in detergent micelles [32] using a systematic DEER analysis of distances between spin label pairs on the extracellular and intracellular sides of the transporter [33]. We identified two conformations of LmrP in equilibrium: outward-facing poised to bind protons and inward-facing from which protons are released. Mapping of the structural rearrangements at basic and acidic pH values established that the protonation state of key acidic residue(s) is the main trigger for the transition between outward-open and inward-open conformations. Specifically a conserved aspartate (D68) was shown to control the energetics of the equilibrium between the two conformations. Residue 68 is part of the signature motif of the MFS [34] and is highly conserved across different organisms [26]. In parallel, a structure of the MFS drug transporter, YajR, identified this residue as a key contributor to the stability of the outward-facing conformation trapped in the crystal [35].

In this work, we show that interactions between lipid headgroups and a conserved network of charges control the proton- and substrate-dependent equilibrium between inward-and outward-facing conformations of LmrP. DEER distance measurements were carried out using selected spin label pairs of the transporter reconstituted in nanodiscs [36] of varying lipid compositions. We found that while the two conformations identified in detergent micelles persists in nanodiscs bilayers, the apparent pK of the conformational transition is shifted by about two pH units. This shift appears to be the consequence of lipid headgroup-dependent stabilization of the inward-facing conformation. To dissect the origin of selective preference for this conformation in lipids, we carried out a systematic mutagenesis of

residues in a charge network hypothesized to modulate the interactions that stabilize the outward-facing conformation. Our data suggest a model in which lipid headgroups interact with this charge network thereby stabilizing an inward-facing conformation.

Results

Conformational dynamics of LmrP in nanodiscs lipid bilayers

We monitored the ligand-dependent conformational changes of LmrP in lipid bilayers by distance measurements of spin labeled cysteine mutants reconstituted into soluble nanoscale phospholipid bilayers (Nanodiscs) [37]. Twelve double cysteines mutants, six on each of the cytoplasmic and extracellular sides of the transmembrane helices (TMs), were selected based on previous results and predictions from homology models [32] (Supplementary Data Sets 1 – 4). On each side, four cysteine pairs probe distances between the N- and C-terminal lobes (Fig. 1), while the other two pairs are located within the same lobe (Supplementary Fig. 1). Following verification of the stability and functional integrity of the mutants (Supplementary Fig. 2 and [32]), they were reconstituted in nanodiscs composed of *E.coli* polar lipids (see Methods) which were previously shown to support proton-coupled transport by LmrP [38,39].

Since LmrP utilizes proton translocation down a transmembrane gradient to power the transport of structurally dissimilar substrates, we studied the structural rearrangements induced by changes in proton concentration (i.e. changes in pH) or following addition of LmrP substrates, either Hoechst 33342 or Ethidium Bromide (EtBr). For this purpose, distance measurements were carried out at pH8 (low proton concentration), pH6 (high proton concentration) and pH8 with substrate. We observed that an increase in proton concentration or addition of Hoechst 33342 results in major structural rearrangements between the N- and C-terminal lobes (Fig. 1). Low pH suppresses the long distance component on the extracellular side (Fig. 1 a), concomitant with a shift in the distributions on the cytoplasmic side (Fig. 1 b). Previous work has shown that such pattern is characteristic of the inward-open/outward-closed state of the transporter [32]. In contrast, the pattern of distance changes observed in the presence of the substrate Hoechst 33342 is opposite to that at low pH demonstrating that substrate binding favors the outward-open (inward-closed) conformation (Fig. 1 a–b).

By comparison, the pairs within the same lobe show minor changes at low pH or upon addition of Hoechst 33342 (Supplementary Fig. 1), with the TM4-TM5 extracellular pair sensitive to pH only (Supplementary Fig. 1 a) and the TM8-TM11 cytoplasmic pair sensitive to Hoechst 33342 only (Supplementary Fig. 1 b). The changes in the distance distribution of these two pairs are likely due to local rearrangements of the spin label(s), as indicated by the alteration of the mobility seen in the CW spectra (Supplementary Data Set 5), and therefore do not reflect backbone rearrangements. We note that the LmrP substrate EtBr barely alters the distance distributions (Supplementary Fig. 3 and Supplementary Fig. 1 c), demonstrating a specificity of the conformational changes to the binding of Hoechst 33342. To demonstrate that EtBr binds LmrP, we carried out distance measurements using the TM10-TM8 pair, previously shown to be sensitive to the presence of bound substrate(s) [32]. In the absence of EtBr, the distance distribution is broad and the peaks are poorly defined. However, in the

presence of EtBr, the distance distribution displays a narrow peak, indicative of a local ordering of LmrP upon substrate binding (Supplementary Fig. 3).

Lipids stabilize the inward-open conformation of LmrP

While the sign and amplitude of the substrate and pH-dependent distance changes are consistent with those previously reported in detergent micelles [32], the presence of the lipids shifts the conformational equilibrium towards the inward-facing conformation at both pH values in figure 1. We note that the reconstitution into nanodiscs has small effects on the average distance for some mutants, suggesting that the conformations in the lipid environment are similar but not necessarily identical.

To investigate the origin of this change in equilibrium between inward-facing and outward-facing states, we systematically compared the pH-dependence of the distance distributions in nanodiscs to that obtained in detergent micelles. We performed distance measurements in the pH range from 4.5 to 8.5 using one distance reporter on each of the extracellular and cytoplasmic sides of the transporter (Fig. 2). The resulting distance distributions for both reporters reveal that, at all pH values, the component(s) characteristic of the inward-open conformation are largely dominant when the transporter is reconstituted into lipids, compared to the transporter in detergent micelles.

To obtain a pH titration curve, the changes in amplitude of the distance components, each representing a conformational state, were quantitatively determined by global analysis of the raw DEER decays for the same spin label pair at different pH values (see Methods). This fitting procedure assumes that the same components (defined by the average distance and the width) are present in each dataset, but their amplitudes are allowed to vary in response to different biochemical conditions (i.e. pH) [40,41]. The resulting titration curve, depicting the population of the inward-open component (Fig. 3) versus pH, has a typical sigmoidal shape with an inflection point at the apparent pK of the transition from one state to the other. On the extracellular side, the apparent pK is 4.7±0.3 for the detergent solubilized protein and increases to 6.9 ±0.2 in nanodiscs of *E.coli* polar lipids (Fig. 3). On the cytoplasmic face, this value is 5.9±0.2 in detergent micelles and 7.3 ±0.1 in the nanodiscs (Fig. 3). Thus, lipids are a determinant of the pH-sensitivity of the global conformational transition of LmrP.

A charge network controls the stability of LmrP conformations

We have previously shown that, in detergent micelles, the pH dependence of the conformational equilibrium is determined to a large extent by the protonation state of the highly conserved residue D68 [32]. A structural interpretation of this result emerged from analysis of the crystal structure of YajR [35], a homolog of LmrP captured in an outward-open conformation. It was observed that this conformation is stabilized by an interaction between the conserved aspartate (residue 73 in YajR) at the cytoplasmic end of helix 2 and the backbone of helix 11 (Fig. 4 a) in the context of a conserved charge-relay network consisting of D73-R77-D126 (D68-R72-D128 in LmrP).

To test if electrostatic interactions in this network of residues contribute to the pH dependence of LmrP conformational change, residues D68 and D128 were mutated to asparagine, in order to mimic protonation. Residue R72 was mutated to a lysine in order to

disrupt the interaction between the guanidinium moiety and D68 and D128 postulated from the YajR structure (Fig. 4 a). We carried out DEER distance measurements on the detergent-solubilized (Supplementary Fig. 4) and nanodisc-reconstituted (Fig. 4) mutants at basic and acidic pH values. In nanodiscs, disruption of the charge-relay network promotes the inward-open conformation regardless of which residue is mutated, as expected from a tightly coupled charge network (Fig. 4 b and c). In contrast to what we observe with the wild-type transporter, addition of Hoechst 33342 to these mutants does not stabilize the outward-open state (Fig. 4 b and c - blue curves).

In detergent micelles, the D68N mutation, but not the D128N and R72K mutations, stabilizes the inward-open conformation at basic pH. The effect of the R72K and D128N mutations only appear at acidic pH (Supplementary Fig. 4). The inequivalence of the charges in detergent micelles suggests that the network is not strongly coupled. Conversely, mutations of the three charges in the lipid environment of nanodiscs have equivalent effects on the relative stability of the conformational states, indicating a strong coupling. These findings underscore the key role of this charge relay in the protonation-dependent conformational switch in LmrP and demonstrate that disruption of this network biases the energy landscape by changing the relative stability of the two conformations.

The effect of the lipids on the conformational equilibrium can be further quantified by comparing the relative ratio of the inward-open and outward-open states to estimate the Gibbs free energy (ΔG°) of the conformational transition either in detergent micelles or nanodisc for each condition tested (see Methods). The changes in ΔG° highlight the dependence of the conformational equilibrium on the charge network and further reinforce the conclusion that the nanodisc bilayer shifts the equilibrium towards the inward-open conformation (Fig. 4 d).

Lipid headgroups modulate the conformational equilibrium

Phosphatidylethanolamine (PE) has been reported to be required for the transport activity of LmrP [42]. We therefore investigated whether the presence of PE can account for the differences in the pH response between detergent and lipids. We performed DEER distance measurements in nanodiscs of defined composition, using synthetic lipids with different polar headgroups.

We first evaluated the potential effects of the fatty acid chain structure on the conformational equilibrium of LmrP by comparing distance distributions in lipids of either i) *E.coli* polar extract, ii) a mixture of 67% PE extracted from *E.coli* (variable fatty acid chains), 23% phosphatidylglycerol (PG) and 10 % cardiolipin (CL) or iii) a mixture of synthetic DOPE (67%) - DOPG (23%) - tetraoleoyl CL (10%). We observed that the structure and length of the fatty acid chain have only minor effects on the distance distributions of the extracellular and cytoplasmic reporters (Fig. 5). Furthermore, the pH- and substrate-dependence of the distance distributions are similar for nanodiscs composed of these different lipid mixtures.

We then investigated whether the headgroup, specifically the methylation state of PE, is important in modulating LmrP conformational equilibrium. For this purpose, we reconstituted the extracellular and cytoplasmic distance reporters in nanodiscs containing PE

with various degree of methylation of the headgroup amine, namely DOPE (no methylation), DOPE(Me)$_2$ (two methylations) and DOPC (fully methylated) while maintaining DOPG at 23% and CL at 10%. Distance distributions obtained at pH5, pH6, pH7 and pH8 uncover a direct correlation between the degree of methylation of the ethanolamine headgroup and the population of the outward-open conformation (Supplementary Fig. 5). To quantitatively assess this effect, we determined ΔG° of the transition between the inward- and outward-facing conformations as a function of pH in each lipid mixture, with the approximation that the transition from inward-open to outward-open conformation is two-state. The raw DEER data were fit using global analysis and the ratios of the populations of the two states were determined and used to calculate ΔG° (Fig. 6).

The methylation of PE headgroup led to stabilization of the outward-open conformation with the strongest effect observed for nanodiscs composed of DOPC-DOPG-CL (Fig. 6 - orange bars). The stabilizing effect of the incremental methylation is enhanced at higher pH: at pH5, the outward-open conformation is not favored in any lipid compositions, while at pH8 it is favored in the DOPE(Me)$_2$-DOPG-CL and DOPC-DOPG-CL nanodiscs. At intermediates pHs, pH6 and pH7, the effects were distinct, suggesting that in this range of pH, the transporter is very sensitive to the presence/absence of protons on the polar headgroup.

Cardiolipin favors closing of the extracellular side

Considering the relative size of the nanodiscs and the transporter, the observed conformational regulation of LmrP by lipids is unlikely to be due to the bulk properties of the bilayer [43]. One possibility is that specific lipid-protein interactions are at play involving select lipids such as PE. One approach to test for such interaction is the identification of endogenous lipid species with high affinity for the target protein. We therefore utilized native mass spectrometry to analyze detergent-solubilized LmrP under increasing voltage which removes the detergent shell [44–46]. At 225 V of collisional activation, the protein is released from its detergent micelle, but still displays substantial spectral heterogeneity (Fig. 7 a). Although little free protein is detected, we observed a distinct pattern, which shows peaks of regular spacing, suggesting the presence of relatively stable lipid-proteins adducts. By gradually increasing the collisional activation from 225 V up to 300 V, the heterogeneity of the protein signal is decreased, due to ejection of the bound lipids, and singly charged species in the mass range around 1440 m/z stand out in the spectrum (Supplementary Fig 6 a). Comparing their masses to a lipid database allowed us to identify these species as a broad range of different CLs, demonstrating a direct interaction between LmrP and this class of lipids with an affinity that withstands detergent solubilization and the energetic conditions required for the MS analysis. Note that the absence of other lipids is not due to the solubilization procedure. Indeed, we determined the lipid species that co-purify with LmrP using quantitative LC-MS/MS analysis (Supplementary Figure 6 b). LmrP-associated micelles contain all *L lactis* lipids, including about 20% of CL demonstrating that the solubilization and purification procedure do not prevent association of a particular lipid species

To elucidate whether the high affinity binding of CL to LmrP modulates the stability of its conformational states, we performed distance measurements on a cytoplasmic and an extracellular distance reporter in a lipid mixture devoid of CL (i.e. DOPE-DOPG) at four different pH values, ranging from pH5 to pH8, as described in the previous section. Remarkably, we observed that the presence of CL affects the conformational equilibrium, but solely on the extracellular side (Fig. 7 b). This is not mediated by a change in the electrostatic surface potential (Supplementary Figure 7) as different ionic strengths (at pH7) did not alter the distance distribution. These findings indicate that the intracellular and extracellular sides of the transporter can rearrange independently, as previously shown [32], and that a specific lipid species—such as CL—might play a local role in the sequence of events leading to a global conformational change.

Discussion

The main finding of this study is that lipid-protein interactions regulate the ion and substrate-dependent conformational dynamics of a secondary transporter. We show that the elements of alternating access are conserved in detergent micelles and the "bilayer-like" environment of nanodiscs: the inward-facing and outward-facing conformations, as defined by patterns of distances between spin labels, are similar and the proton-dependent switch is maintained [32]. However, the presence of lipids shapes the energetics of alternating access by altering the relative stability of the two conformations. Whereas relatively acidic pH values were required to observe the distance peak(s) characteristic of the inward-open conformation in detergent micelles, the same peak(s) are present at neutral to basic pH in nanodiscs. Consequently, the apparent pK of the conformational transition is shifted towards neutral pH in nanodiscs. As *L. lactis* typically thrives in pH range 6–7 [47,48], the lipid environment would enable the coexistence of the conformational intermediates at pH values closer to physiological pH. Conversely, the conformational transition would be very unlikely under physiological conditions if the pK is close to the acidic values observed in detergent.

Lipid headgroups modulate LmrP's conformational landscape

Our data unequivocally reveals a dependence of the equilibrium between inward-facing and outward-facing conformations on the headgroup of surrounding phospholipids. In particular, PE was shown to selectively stabilize the inward-facing conformation while CL promotes the uncoupled closing of the extracellular side. How might this change in relative stability of conformers be achieved?

Insight into the mechanism by which PE shifts the conformational equilibrium was obtained from the finding that the systematic substitution of the amine protons by methyl groups favors the outward-open conformation, suggesting a direct coupling between the availability of protons on the headgroup and the shift in equilibrium. One interpretation of this result is that direct hydrogen bond(s) between the headgroup and the transporter plays a role in the conformational regulation. Such modulation of the conformational equilibrium through direct hydrogen bonding with the phospholipids has been suggested for other membrane transport proteins such as the lactose permease LacY [49], the branched chain amino acid transport system from *S.cremoris* [50], the mechanosensitive channel MscL [51], and LmrP

itself [42]. However, we cannot exclude a more indirect effect. The size difference between the headgroups might cause local changes in the lateral pressure that could play a role in modulating the relative stability of the different states and thus in the conformational equilibrium.

Despite its effect on the energetics of LmrP conformational equilibrium, no high affinity bound PE was identified by native MS. Rather, these measurements revealed the presence of several molecules of CL bound to LmrP, indicating a specific interaction. Remarkably, binding of CL was correlated with a direct structural effect manifested by the closing of the extracellular side independent of an apparent movement on the intracellular side.

Extensive studies have explored the role of CL in the regulation of transporter function and pointed out its implication in the bioenergetics of the cell. CL displays increased affinity for all membrane proteins involved in ATP synthesis in the mitochondrion of eukaryotes and the plasma membrane of prokaryotes (reviewed in [52]). In addition, CL molecules are often observed in the crystal structures of mitochondrial membrane proteins [53–55] and have been suggested to take an active part in proton uptake [56,57]. Early studies assigned a pKa_2 of ~7 to one of the phosphate groups, a value that would allow CL to play a role as a versatile proton donor/acceptor and bind protons from the extracellular side [58,59]. Although the physiological roles of this unusual lipid continue to be elusive, the observation that high affinity interaction with CL is associated with closing of the extracellular side of LmrP is consistent with a proton donor role for this lipid, which would facilitate the protonation of acidic residues.

A charge network likely mediates LmrP-lipid interactions

Based on the structure of the multidrug transporter YajR (Fig. 4 a), the interaction between the conserved Asp73 (Asp68 in LmrP) and the backbone of helix 11 appears to stabilize the outward-open conformation. This contention is supported by the changes observed in the distances distributions upon D68 mutation (Fig. 4 and Supplementary Fig. 4), which consistently favors the inward-open conformation independent of the biochemical conditions (pH and/or lipids).

One possibility is that the lipid-mediated shift in the equilibrium towards the inward-open state reflects an increase in the pK_a of D68 that is caused by a direct interaction between the phospholipid headgroup and the regulatory motif. This model is consonant with a number of evidence including the recent demonstration of conformational rearrangements of the ammonia transporter AmtB as a consequence of a direct interaction between a motif and PG bound with high-affinity [15]. Furthermore, a direct interaction through hydrogen bonding between PE headgroup and the aspartate 68 has already been suggested for the MFS symporter LacY based on computational studies in lipid bilayers composed of PE with various degree of methylation [60]. Functional studies carried out on LmrP D68C mutant reconstituted in proteoliposomes of various lipid compositions led to a similar conclusion [42]. Nevertheless, considering the topological asymmetry between the outward-open and inward-open state, indirect effects such as lateral pressure may be involved in the conformational regulation as well.

The YajR structure shows that the key aspartate is positioned to participate in a charge relay with two conserved residues, arginine 77 and aspartate 126, in addition to its interaction with TM11 (Fig. 4 a). Therefore, the lipid-mediated stabilization of the inward-facing conformation of LmrP could involve a specific interaction between the aspartate 68, the charge relay and the headgroup that weakens the interaction with TM11. Our data indicate that the coupling between the residues of the charge relay motif is stronger in a lipid environment, supporting the hypothesis of an extended network involving a lipid headgroup. In contrast, detergent micelles would favor the interaction of D68 with TM11 at high pH thus explaining the lack of effects of R72K and D128N mutations on the conformational equilibrium at basic pH. We conclude that a balance between lipid-protein interactions and intra-protein interactions regulates the conformational equilibrium of LmrP.

Concluding remarks

Our work provides a perspective on the role of lipids in the conformational dynamics of a membrane transporter, and thereby emphasizes that interactions with the membrane are a key determinant that has to be accounted for in the elucidation of the mechanism(s) of transporters. The model that emerges from our data hypothesizes a direct interaction of lipid headgroups with charged residues to modulate the energetic of alternating access. Whether or not this mechanism can be extended to other transporters energized by a proton gradient remains to be investigated. We surmise that the strategy used here, where intramolecular distances are measured in detergent and in nanodiscs at various pH values, can be applied to a variety of such systems in order to test the role of lipid-protein interactions.

Online Methods

LmrP homology models

For each of the four structural templates (EmrD, PDB entry: 2GFP [61], LacY PDB: 2V8N [62], FucP PDB: 3O7Q [63] and YajR PDB: 3WDO [35]), the sequence of LmrP was aligned using multiple alignments of LmrP and orthologs together with the sequences of the template and its orthologs. Initial alignments were generated using ClustalW [64], and then manually adjusted to i) prevent insertion and deletion in the TM helices and ii) avoid introduction of charged residues facing the lipid tails. Subsequent LmrP-template sequence alignments were then used to generate molecular models with Modeller [65]. The homology models based on EmrD, LacY, FucP and YajR are available as Supplementary Data Sets 1, 2, 3 and 4 respectively. Figures were prepared with Chimera [66].

Design and construction of the mutants

Cysteine-replacement residues were selected to be located at the extracellular or cytoplasmic end of a chosen TM region by using the homology models, while avoiding mutation of conserved residues. The mutations were introduced in C-terminally His-tagged LmrP in a derivative of the *E.coli* PCR®4 Blunt-TOPO® vector (Invitrogen) by site-directed mutagenesis using the QuikChange Lightning kit (Stratagene). The endogenous cysteine 270 was previously replaced by an alanine using the same method. After transformation, plasmid DNA was extracted and verified by sequencing. The *lmrp* gene fragment containing the desired mutation was then introduced into the pHLP5-3C vector, a derivative of the *L. lactis*

expression vector pHLP5 containing C-terminally His-tagged LmrP [38]. After electroporation into NZ9000 *L. lactis* cells, the sequence was verified once again.

Bacterial strains, plasmids and growth conditions

The *L. lactis* NZ9000 was used as a host for pHLP5-3C based plasmid expression, as described previously [42,67,68]. Briefly, cells were grown at 30 °C in M17 medium supplemented with 0.5 % glucose and 5 $mg.mL^{-1}$ chloramphenicol until the OD_{660} reached 0.8. Overexpression of LmrP mutants was then induced by addition of 1:1000 dilution of the supernatant of the nisin producing *L. lactis* strain NZ9700 [69]. After 2 hours of induction, cells were harvested by centrifugation at 5,000×*g*

LmrP mutants purification and labeling

Cells were washed in 50 mM HEPES, pH7 and resuspended (10 mL for each L of culture) in the same buffer containing 5 $mg.mL^{-1}$ of lysozyme, 10 $\mu g.mL^{-1}$ of DNAse I and 10 mM of $MgSO_4$. After 1-hour incubation at 30 °C, cells were broken by four passes at ~15,000 psi using a high pressure homogenizer. Cell debris and undisrupted cells were subsequently removed by three 15min centrifugations at 14,000×*g*. Inside-out membrane vesicles were then isolated by ultracentrifugation at 125,000×*g* for 2.5h at 4 °C and resuspended in 50 mM HEPES pH7, 150 mM NaCl and 10 % (v/v) glycerol (10 mL per L of cells). Inside-out membrane vesicles were solubilized with 1.2 % (w/v) β-dodecylmaltoside in the presence of 1 mM DTT for 1.5h at 4 °C on a rotating wheel. The insoluble fraction was then removed by ultracentrifugation at 125,000×*g* for 1h and the supernatant was batch-incubated for 2h with previously equilibrated Ni-NTA resin (25 μL resin per mL supernatant) in the presence of 10 mM imidazole. The slurry was then transferred to a column, the flow-through discarded, and the resin washed with 8 volumes of buffer A (50 mM HEPES pH7, 100 mM NaCl, 0.05 % (w/v) β-DDM and 20 mM imidazole), after which the protein was eluted by stepwise addition of buffer B (buffer A containing 250 mM imidazole). The concentration of the protein was determined by UV absorbance measurement at 280 nm. Spin-labeling was performed by adding a 30-fold molar excess of MTSSL (Enzo Life Sciences) from a 100 μM stock solution in DMF. The reaction was kept in the dark and at room temperature for 2h, and the process was repeated, followed by overnight incubation on ice. The protein was then run on a Superdex-200 (GE Healthcare) size-exclusion chromatography column in HEPES buffer (50 mM HEPES pH8, 150 mM NaCl, 10 % (v/v) glycerol and 0.02 % (w/v) β-DDM).

MSP1E3D1 production and purification

Membrane scaffold protein (MSP1D1E3) was expressed and purified as described earlier [41,70] with the following modifications. Briefly, *E.coli* BL21 (DE3) cells containing the MSP1D1E3 gene in pET-28a(+) were plated on LB-agar plates supplemented with kanamycin (30 $\mu g.mL^{-1}$). A single colony was used to inoculate 30 mL of LB supplemented with 30 $\mu g.mL^{-1}$ of kanamycin. A dense overnight culture of 30 mL was used to inoculate secondary culture of 1L Terrific broth supplemented with 30 $\mu g.mL^{-1}$ of kanamycin. Cultures were grown at 37°C with shaking to an OD_{600} of ~2.2–2.5, then the expression of MSP1D1E3 was induced by addition of 1 mM IPTG (Inalco). Cultures were further grown for 4h at 37°C, and cells were harvested by centrifugation. Cell pellets were resuspended in 30 mL of lysis buffer (20 mM sodium phosphate, 1% Triton X-100, pH7.4), including 1/3 of

a Complete EDTA-free protease inhibitor cocktail tablet (Roche), 10 μg.mL^{-1} of DNase I, and 10 mM of $MgSO_4$, and were lysed by 4 passes at 15000 psi in a high pressure homogenizer (Emulsiflex®). The lysate was centrifuged at 30,000×*g* for 30 min, and the supernatant was mixed with 3 mL of Ni-NTA resin equilibrated with lysis buffer. The slurry was transferred to a column and the flow-through discarded. The resin was washed with four bed volumes of buffer A (40 mM Tris/HCl, 0.3 M NaCl, pH8.0) containing 1% Triton X-100, four bed volumes of buffer A containing 50 mM sodium cholate, four bed volumes of buffer A containing 20 mM imidazole, four bed volumes of buffer A containing 50 mM imidazole. The bound protein was eluted step-wise with buffer A containing 300 mM imidazole. The eluted MSP1D1E3 was passed over a desalting column into MSP buffer (50 mM Tris/HCl, 0.1M NaCl, 0.5 mM EDTA, pH7.5) and the concentration was determined by absorbance at 280 nm (extinction coefficient = 29,910 M^{-1} cm^{-1}). The protein was concentrated to ~15 mg.mL^{-1} on 10K MWCO concentrator (Amicon). The purity was assessed by SDS-PAGE and Coomassie staining.

Lipids preparation for nanodiscs

Lipids dissolved in chloroform (Avanti polar lipids) were combined to reach a final quantity of 100 mg, dried under nitrogen flow and then desiccated overnight under vacuum. The lipid films were hydrated with MSP buffer to reach a final concentration of 40 mg.mL^{-1}. β-DDM was added to the mixture to reach a final concentration of 7.5% (w/v). The lipids were further homogenized by low power sonication (160W) in Bioruptor ® for 5 min, with 30s ON - 30s OFF cycles, aliquoted and stored at −80 °C.

Reconstitution of LmrP in nanodiscs

For reconstitution into nanodiscs, spin-labeled LmrP mutants in β-DDM micelles were mixed with the appropriate lipid mixture, MSP1D1E3 and β-DDM in the following molar ratios:lipid:MSP1D1E3, 60:1; MSP1D1E3:LmrP, 8:1; β -DDM:lipid, 3:1. Mixtures were rocked at room temperature for 30 min then incubated overnight at 4°C with rocking. In the morning, Biobeads SM-2 (700 mg.mL^{-1}) (Biorad) were added to the mixture, and incubated for 2h at 4°C then 1h at RT. The removal of the Biobeads was achieved by low speed centrifugation of the eppendorf containing the nanodisc assembly perforated with a needle to form a tiny hole. Nanodiscs were purified from undesirable species by size-exclusion chromatography on a superdex200 column (GE). Nanodiscs were concentrated using Amicon Ultra-50K centrifugal filter units at a speed not exceeding 1000*xg*. Nanodiscs containing the LmrP mutants were then characterized using SDS-PAGE to verify reconstitution and estimate reconstitution efficiency. As a complementary measurement, concentration of spin-labeled mutants in nanodiscs was determined as described previously [36] by comparing the intensity of the integrated CW-EPR spectrum to that of the same mutant in detergent micelles. The reconstitution efficiency was estimated to be 30%.

Preparation of the sample for DEER measurements

The protein in detergent micelles or reconstituted in nanodiscs was concentrated using a 50K MWCO concentrator to a spin label concentration of 100–150 μM (determined by the integration of the CW spectrum) after which glycerol was added to a final concentration of 23 % (v/v). For measurements performed at pHs other than pH8, two strategies were used.

For the detergent-solubilized protein, an additional run on a desalting column was performed after size-exclusion chromatography and prior to concentration in order to exchange the buffer from HEPES pH8 to the appropriate buffer set at the right pH (MES-acetate 50 mM buffer for acidic pH values). Another strategy had to be used for the nanodiscs samples, as they tend to be unstable under acidic conditions and could not be concentrated as such. Consequently, an appropriate amount of acetic acid at 0.5M was added to the concentrated sample to lower its pH, which was checked with pH-paper. Where appropriate, Hoechst 33342 or Ethidium Bromide was added to a final concentration of 1 mM.

EPR measurements

DEER measurements were performed on a Bruker 580 pulsed ESR spectrometer operating at Q-band (33.4 GHz) using a standard four pulse protocol [71–73]. Data was collected with the samples at 83 K with 23 % (v/v) glycerol as cryoprotectant. Analysis of the DEER data to determine the distance distributions was carried in DeerAnalysis2011 or DeerAnalysis2013 [74]. The data was fit with Tikhonov regularization and L-curve determination of the optimal regularization parameter. Optimal background correction was established by statistical analysis of the fits. The acquisition time was optimized for each spin pair. Please note that the distance distributions are accurate up to 45 Å for data recorded for 2 μs and up to 54 Å for data recorded for 2.5 μs. For a few samples, we observed evidence of partial protein aggregation [72]. This was manifested in the raw DEER decays by a deviation of the baseline from a stretched exponential and the lack of an oscillation in the echo decay even at longer collection times. Aggregation results in a component at the tail end of the distance distribution. The artifactual nature of these peaks (marked with an asterisk) could thus be demonstrated by varying the measured duration of the echo intensity oscillation. For the combined analysis of the DEER data a home-written software operating in the Matlab environment was used [40,41,75]. The software assumes that the distance distribution consists of a sum of Gaussians and that the amplitudes of the components are allowed to vary across the physiological conditions, e.g. pH and lipid composition. The software has been deposited in the MATLAB file exchange (http://www.mathworks.com/matlabcentral/fileexchange/46729-deera2012-zip/content/DeerA.m). The binding curves were analyzed and fitted using Origin. For the ΔG° calculation, the amplitudes of the fits that describe the outward facing or inward facing structures are obtained. The two amplitudes are then compared to obtain a K_{eq} for the two states for each pH and lipid condition. The K_{eq}'s are then used to obtain the ΔG°. The error bars are obtained by propagating the fit errors for the individual amplitudes. The analysis of the raw DEER data is presented on Supplementary Data Sets 6 and 7.

Native MS measurements

Purified LmrP in detergent micelles was buffer exchanged into 100 mM ammonium acetate buffer pH6.8 supplemented with 0.02% n-dodecyl-β-D-maltoside using a G25 Sephadex column (GE lifesciences). Samples were introduced into the vacuum of the mass spectrometer using nano-electrospray ionization with in-house prepared gold-coated borosilicate glass capillaries using a spray voltage of +1.6 kV. Spectra were recorded on a quadrupole TOF instrument (Q-TOF2, Waters, Manchester, UK) modified for transmission of native, high m/*z* protein assemblies, as described elsewhere [76]. Critical voltages and

pressures throughout the instrument were 100 V and 225 V for the sampling cone and collision voltage respectively, with pressures of 15 and $2E^{-2}$ mbar for the source and collision cell. For the identification of the CL lipids a Synapt G2 (Waters, Manchester, UK) instrument was used due to the increased mass resolution at lower m/*z* values. Critical settings were sampling cone 200 V, 200 V trap collision energy, 10 V trap DC bias and 75 transfer collision energy. Pressures throughout the instrument were 6.5 and 2.6 E^{-2} mbar for the source and trap/transfer collision cells. All spectra were processed using Masslynx v4.1 (Waters).

LC-MS/MS identification and quantification of lipids

Lipid extraction and mass spectrometry analysis of lipids from purified LmrP was performed as following. Standards for each phospholipid class were added to 1–2mg purified LmrP and lipids were then extracted from membranes by methanol/chloroform extraction as described in [77] with the following modifications: 10mL HCl 6N were added to the mixture and extraction was repeated 3 times on the same sample to have maximum recovery of all types of lipids; corresponding organic phases were pooled together, the solvent evaporated under nitrogen stream and lipids then dissolved in dichloromethane:Isopropanol (1:4) prior to mass spectrometry analysis. Samples were injected in a rapid resolution liquid chromatography system (RRLC 1200 series from Agilent Technologies, CA, USA) fitted with a XDB Eclipse Plus C18, 4.6×150 mm, 1.8 mm. A 6520 series electrospray ion source (ESI) - quadrupole time-of-flight (Q-TOF) from Agilent Technologies was used for the MS/MS analyses in positive and negative mode. For quantification, single MS analyses were performed. All data were acquired by the Mass Hunter Acquisition® (Agilent Technologies). For data analysis, first fragment based searching mode analysis by Mass Hunter Qualitative Analysis® (Agilent Technologies, CA, USA) was applied on MS/MS spectra in positive and negative mode to identify lipid species. Then for quantification, samples were run in simple MS mode. Extracted ion chromatograms were extracted based on the exact masses of the lipids observed during auto MSMS analyses. Phospholipids were quantified by the standard curves run during the set of experiments.

Transport assay

The transport activity of the LmrP mutants was assayed as described previously [68,78]. Briefly, inside-out membrane vesicles of LmrP-expressing cells (~ 1 mg of LmrP) were incubated 5 min in transport buffer (50 mM HEPES, 2 mM $MgCl_2$, 300 mM KCl, pH7.4) at 30 °C in the presence of 0.1 μM Hoechst 33342. Addition of 2 mM Mg^{2+}-ATP allowed to generate a proton-motive force by activating the endogenous F0/F1 H^+ - ATPase, thereby initiating LmrP transport activity. Fluorescence spectroscopy (EX 355 nm, EM 457 nm) was used to measure the rate of extrusion of the substrate Hoechst 33342 (Invitrogen) out of the membrane. The decrease of Hoechst 33342 fluorescence over time as a result of its extrusion from the membrane reports LmrP transport activity.

Supplementary Material

Refer to Web version on PubMed Central for supplementary material.

Acknowledgments

We thank D. Claxton, R. Dastvan and D. Hilger for critically reading the manuscript, V. Debruycker for providing the solubilized protein used for the MS measurements and JM. Ruysschaert for helpful discussions.

This work was supported by the Fonds de la Recherche Scientifique F.R.S.-F.N.R.S. (grant F.4523.12 - to C.G) and the NIH (grant R01GM077659 - to H.S.M)

C.M. is supported as a Research Fellow of the F.R.I.A

C.G. is supported as a Research Associate of the F.R.S.-F.N.R.S and a Welbio Investigator.

References

1. Singer SJ, Nicolson GL. The fluid mosaic model of the structure of cell membranes. Science. 1972; 175:720–731. [PubMed: 4333397]
2. Heijne G. The distribution of positively charged residues in bacterial inner membrane proteins correlates with the trans-membrane topology. EMBO J. 1986; 5:3021–3027. [PubMed: 16453726]
3. Cantor RS. The influence of membrane lateral pressures on simple geometric models of protein conformational equilibria. Chem Phys Lipids. 1999; 101:45–56. [PubMed: 10810924]
4. Powl AM, East JM, Lee AG. Anionic phospholipids affect the rate and extent of flux through the mechanosensitive channel of large conductance MscL. Biochemistry. 2008; 47:4317–4328. [PubMed: 18341289]
5. Phillips R, Ursell T, Wiggins P, Sens P. Emerging roles for lipids in shaping membrane-protein function. Nature. 2009; 459:379–385. [PubMed: 19458714]
6. Dowhan W, Bogdanov M. Lipid-protein interactions as determinants of membrane protein structure and function. Biochem Soc Trans. 2011; 39:767–774. [PubMed: 21599647]
7. Hanson MA, et al. A specific cholesterol binding site is established by the 2.8 A structure of the human beta2-adrenergic receptor. Structure. 2008; 16:897–905. [PubMed: 18547522]
8. Hunte C, Richers S. Lipids and membrane protein structures. Curr Opin Struct Biol. 2008; 18:406–411. [PubMed: 18495472]
9. Lee AG. Lipid-protein interactions in biological membranes: a structural perspective. Biochim Biophys Acta. 2003; 1612:1–40. [PubMed: 12729927]
10. Ellena JF, Blazing MA, McNamee MG. Lipid-protein interactions in reconstituted membranes containing acetylcholine receptor. Biochemistry. 1983; 22:5523–5535. [PubMed: 6317021]
11. Fernandez-Ballester G, et al. Role of cholesterol as a structural and functional effector of the nicotinic acetylcholine receptor. Biochem Soc Trans. 1994; 22:776–780. [PubMed: 7821683]
12. Contreras FX, et al. Molecular recognition of a single sphingolipid species by a protein's transmembrane domain. Nature. 2012; 481:525–529. [PubMed: 22230960]
13. Lee AG. Lipid-protein interactions. Biochem Soc Trans. 2011; 39:761–766. [PubMed: 21599646]
14. Vitrac H, Bogdanov M, Dowhan W. Proper fatty acid composition rather than an ionizable lipid amine is required for full transport function of lactose permease from Escherichia coli. J Biol Chem. 2013; 288:5873–5885. [PubMed: 23322771]
15. Laganowsky A, et al. Membrane proteins bind lipids selectively to modulate their structure and function. Nature. 2014; 510:172–175. [PubMed: 24899312]
16. Pliotas C, et al. The role of lipids in mechanosensation. Nat Struct Mol Biol. 2015; 22:991–998. [PubMed: 26551077]
17. Koshy C, et al. Structural evidence for functional lipid interactions in the betaine transporter BetP. EMBO J. 2013; 32:3096–3105. [PubMed: 24141878]
18. Dawaliby R, et al. Allosteric regulation of G protein-coupled receptor activity by phospholipids. Nat Chem Biol. 2015
19. Hamilton PJ, et al. PIP2 regulates psychostimulant behaviors through its interaction with a membrane protein. Nature Chemical Biology. 2014; 10:582–589. [PubMed: 24880859]

20. Khelashvili G, Weinstein H. Functional mechanisms of neurotransmitter transporters regulated by lipid-protein interactions of their terminal loops. Biochimica Et Biophysica Acta-Biomembranes. 2015; 1848:1765–1774.
21. Khelashvili G, Galli A, Weinstein H. Phosphatidylinositol 4,5-Biphosphate (PIP2) Lipids Regulate the Phosphorylation of Syntaxin N-Terminus by Modulating Both Its Position and Local Structure. Biochemistry. 2012; 51:7685–7698. [PubMed: 22950482]
22. Sachs JN, Engelman DM. Introduction to the membrane protein reviews: the interplay of structure, dynamics, and environment in membrane protein function. Annu Rev Biochem. 2006; 75:707–712. [PubMed: 16756508]
23. Bolhuis H, et al. Energetics and mechanism of drug transport mediated by the lactococcal multidrug transporter LmrP. J Biol Chem. 1996; 271:24123–24128. [PubMed: 8798651]
24. Putman M, van Veen HW, Degener JE, Konings WN. The lactococcal secondary multidrug transporter LmrP confers resistance to lincosamides, macrolides, streptogramins and tetracyclines. Microbiology. 2001; 147:2873–2880. [PubMed: 11577166]
25. Gottesman MM, Pastan I. Biochemistry of multidrug resistance mediated by the multidrug transporter. Annu Rev Biochem. 1993; 62:385–427. [PubMed: 8102521]
26. Putman M, van Veen HW, Konings WN. Molecular properties of bacterial multidrug transporters. Microbiol Mol Biol Rev. 2000; 64:672–693. [PubMed: 11104814]
27. Fluman N, Ryan CM, Whitelegge JP, Bibi E. Dissection of mechanistic principles of a secondary multidrug efflux protein. Mol Cell. 2012; 47:777–787. [PubMed: 22841484]
28. Schaedler TA, van Veen HW. A flexible cation binding site in the multidrug major facilitator superfamily transporter LmrP is associated with variable proton coupling. FASEB J. 2010; 24:3653–3661. [PubMed: 20472749]
29. Schuldiner S. EmrE, a model for studying evolution and mechanism of ion-coupled transporters. Biochim Biophys Acta. 2009; 1794:748–762. [PubMed: 19167526]
30. Paulsen IT, Brown MH, Littlejohn TG, Mitchell BA, Skurray RA. Multidrug resistance proteins QacA and QacB from Staphylococcus aureus: membrane topology and identification of residues involved in substrate specificity. Proc Natl Acad Sci U S A. 1996; 93:3630–3635. [PubMed: 8622987]
31. Kaatz GW, Seo SM. Inducible NorA-mediated multidrug resistance in Staphylococcus aureus. Antimicrob Agents Chemother. 1995; 39:2650–2655. [PubMed: 8592996]
32. Masureel M, et al. Protonation drives the conformational switch in the multidrug transporter LmrP. Nat Chem Biol. 2014; 10:149–155. [PubMed: 24316739]
33. Claxton DP, Kazmier K, Mishra S, McHaourab HS. Navigating Membrane Protein Structure, Dynamics, and Energy Landscapes Using Spin Labeling and EPR Spectroscopy. Methods Enzymol. 2015; 564:349–387. [PubMed: 26477257]
34. Pao SS, Paulsen IT, Saier MH Jr. Major facilitator superfamily. Microbiol Mol Biol Rev. 1998; 62:1–34. [PubMed: 9529885]
35. Jiang D, et al. Structure of the YajR transporter suggests a transport mechanism based on the conserved motif A. Proc Natl Acad Sci U S A. 2013; 110:14664–14669. [PubMed: 23950222]
36. Zou P, McHaourab HS. Increased sensitivity and extended range of distance measurements in spin-labeled membrane proteins: Q-band double electron-electron resonance and nanoscale bilayers. Biophys J. 2010; 98:L18–L20. [PubMed: 20303847]
37. Bayburt TH, Sligar SG. Self-assembly of single integral membrane proteins into soluble nanoscale phospholipid bilayers. Protein Sci. 2003; 12:2476–2481. [PubMed: 14573860]
38. Putman M, van Veen HW, Poolman B, Konings WN. Restrictive use of detergents in the functional reconstitution of the secondary multidrug transporter LmrP. Biochemistry. 1999; 38:1002–1008. [PubMed: 9893996]
39. Gbaguidi B, et al. Proton motive force mediates a reorientation of the cytosolic domains of the multidrug transporter LmrP. Cell Mol Life Sci. 2004; 61:2646–2657. [PubMed: 15526169]
40. Stein RA, Beth AH, Hustedt EJ. A Straightforward Approach to the Analysis of Double Electron-Electron Resonance Data. Methods Enzymol. 2015; 563:531–567. [PubMed: 26478498]
41. Mishra S, et al. Conformational dynamics of the nucleotide binding domains and the power stroke of a heterodimeric ABC transporter. Elife. 2014; 3:e02740. [PubMed: 24837547]

42. Hakizimana P, Masureel M, Gbaguidi B, Ruysschaert JM, Govaerts C. Interactions between phosphatidylethanolamine headgroup and LmrP, a multidrug transporter: a conserved mechanism for proton gradient sensing? J Biol Chem. 2008; 283:9369–9376. [PubMed: 18234676]
43. Denisov IG, McLean MA, Shaw AW, Grinkova YV, Sligar SG. Thermotropic phase transition in soluble nanoscale lipid bilayers. J Phys Chem B. 2005; 109:15580–15558. [PubMed: 16852976]
44. Lanucara F, Holman SW, Gray CJ, Eyers CE. The power of ion mobility-mass spectrometry for structural characterization and the study of conformational dynamics. Nat Chem. 2014; 6:281–294. [PubMed: 24651194]
45. Zhou M, et al. Mass spectrometry of intact V-type ATPases reveals bound lipids and the effects of nucleotide binding. Science. 2011; 334:380–385. [PubMed: 22021858]
46. Bechara C, et al. A subset of annular lipids is linked to the flippase activity of an ABC transporter. Nat Chem. 2015; 7:255–262. [PubMed: 25698336]
47. Adamberg K, Kask S, Laht TM, Paalme T. The effect of temperature and pH on the growth of lactic acid bacteria: a pH-auxostat study. Int J Food Microbiol. 2003; 85:171–183. [PubMed: 12810281]
48. Bibal B, Goma G, Vayssier Y, Pareilleux A. Influence of Ph, Lactose and Lactic-Acid on the Growth of Streptococcus-Cremoris - a Kinetic-Study. Applied Microbiology and Biotechnology. 1988; 28:340–344.
49. Chen CC, Wilson TH. The phospholipid requirement for activity of the lactose carrier of Escherichia coli. J Biol Chem. 1984; 259:10150–10158. [PubMed: 6381481]
50. Driessen AJ, Zheng T, In't Veld G, Op den Kamp JA, Konings WN. Lipid requirement of the branched-chain amino acid transport system of Streptococcus cremoris. Biochemistry. 1988; 27:865–872. [PubMed: 3284574]
51. Powl AM, East JM, Lee AG. Importance of direct interactions with lipids for the function of the mechanosensitive channel MscL. Biochemistry. 2008; 47:12175–12184. [PubMed: 18950196]
52. Haines TH. A new look at Cardiolipin. Biochim Biophys Acta. 2009; 1788:1997–2002. [PubMed: 19801076]
53. Shintre CA, et al. Structures of ABCB10, a human ATP-binding cassette transporter in apo-and nucleotide-bound states. Proc Natl Acad Sci U S A. 2013; 110:9710–9715. [PubMed: 23716676]
54. Nury H, et al. Structural basis for lipid-mediated interactions between mitochondrial ADP/ATP carrier monomers. FEBS Lett. 2005; 579:6031–6036. [PubMed: 16226253]
55. Ruprecht JJ, et al. Structures of yeast mitochondrial ADP/ATP carriers support a domain-based alternating-access transport mechanism. Proc Natl Acad Sci U S A. 2014; 111:E426–E434. [PubMed: 24474793]
56. Lange C, Nett JH, Trumpower BL, Hunte C. Specific roles of protein-phospholipid interactions in the yeast cytochrome bc1 complex structure. EMBO J. 2001; 20:6591–6600. [PubMed: 11726495]
57. Poyry S, et al. Atomistic simulations indicate cardiolipin to have an integral role in the structure of the cytochrome bc(1) complex. Biochimica Et Biophysica Acta-Bioenergetics. 2013; 1827:769–778.
58. Kates M, Syz JY, Gosser D, Haines TH. pH-dissociation characteristics of cardiolipin and its 2'-deoxy analogue. Lipids. 1993; 28:877–882. [PubMed: 8246687]
59. Haines TH, Dencher NA. Cardiolipin: a proton trap for oxidative phosphorylation. FEBS Lett. 2002; 528:35–39. [PubMed: 12297275]
60. Lensink MF, Govaerts C, Ruysschaert JM. Identification of specific lipid-binding sites in integral membrane proteins. J Biol Chem. 2010; 285:10519–10526. [PubMed: 20139086]

References for Online Methods

61. Yin Y, He X, Szewczyk P, Nguyen T, Chang G. Structure of the multidrug transporter EmrD from Escherichia coli. Science. 2006; 312:741–744. [PubMed: 16675700]
62. Guan L, Mirza O, Verner G, Iwata S, Kaback HR. Structural determination of wild-type lactose permease. Proc Natl Acad Sci U S A. 2007; 104:15294–15298. [PubMed: 17881559]

63. Dang S, et al. Structure of a fucose transporter in an outward-open conformation. Nature. 2010; 467:734–738. [PubMed: 20877283]
64. Thompson JD, Higgins DG, Gibson TJ. CLUSTAL W: improving the sensitivity of progressive multiple sequence alignment through sequence weighting, position-specific gap penalties and weight matrix choice. Nucleic Acids Res. 1994; 22:4673–4680. [PubMed: 7984417]
65. Webb B, Sali A. Comparative Protein Structure Modeling Using MODELLER. Curr Protoc Bioinformatics. 2014; 47:561–556.
66. Pettersen EF, et al. UCSF Chimera--a visualization system for exploratory research and analysis. J Comput Chem. 2004; 25:1605–1612. [PubMed: 15264254]
67. Mazurkiewicz P, Driessen AJ, Konings WN. Energetics of wild-type and mutant multidrug resistance secondary transporter LmrP of Lactococcus lactis. Biochim Biophys Acta. 2004; 1658:252–261. [PubMed: 15450963]
68. Putman M, Koole LA, van Veen HW, Konings WN. The secondary multidrug transporter LmrP contains multiple drug interaction sites. Biochemistry. 1999; 38:13900–13905. [PubMed: 10529235]
69. Mierau I, Kleerebezem M. 10 years of the nisin-controlled gene expression system (NICE) in Lactococcus lactis. Appl Microbiol Biotechnol. 2005; 68:705–717. [PubMed: 16088349]
70. Boldog T, Li M, Hazelbauer GL. Using Nanodiscs to create water-soluble transmembrane chemoreceptors inserted in lipid bilayers. Methods Enzymol. 2007; 423:317–335. [PubMed: 17609138]
71. Jeschke G, Polyhach Y. Distance measurements on spin-labelled biomacromolecules by pulsed electron paramagnetic resonance. Phys Chem Chem Phys. 2007; 9:1895–1910. [PubMed: 17431518]
72. Jeschke G. DEER distance measurements on proteins. Annu Rev Phys Chem. 2012; 63:419–446. [PubMed: 22404592]
73. Pannier M, Veit S, Godt A, Jeschke G, Spiess HW. Dead-time free measurement of dipole-dipole interactions between electron spins. J Magn Reson. 2000; 142:331–340. [PubMed: 10648151]
74. Jeschke G, et al. DeerAnalysis2006—a comprehensive software package for analyzing pulsed ELDOR data. Applied Magnetic Resonance. 2006; 30:473–498.
75. Brandon S, Beth AH, Hustedt EJ. The global analysis of DEER data. J Magn Reson. 2012; 218:93–104. [PubMed: 22578560]
76. Sobott F, Hernandez H, McCammon MG, Tito MA, Robinson CV. A tandem mass spectrometer for improved transmission and analysis of large macromolecular assemblies. Anal Chem. 2002; 74:1402–1407. [PubMed: 11922310]
77. Bligh EG, Dyer WJ. A rapid method of total lipid extraction and purification. Can J Biochem Physiol. 1959; 37:911–917. [PubMed: 13671378]
78. Steed PR, Zou P, Trone KE, McHaourab HS. Structure and pH-induced structural rearrangements of the putative multidrug efflux pump EmrD in liposomes probed by site-directed spin labeling. Biochemistry. 2013; 52:7964–7974. [PubMed: 24148002]

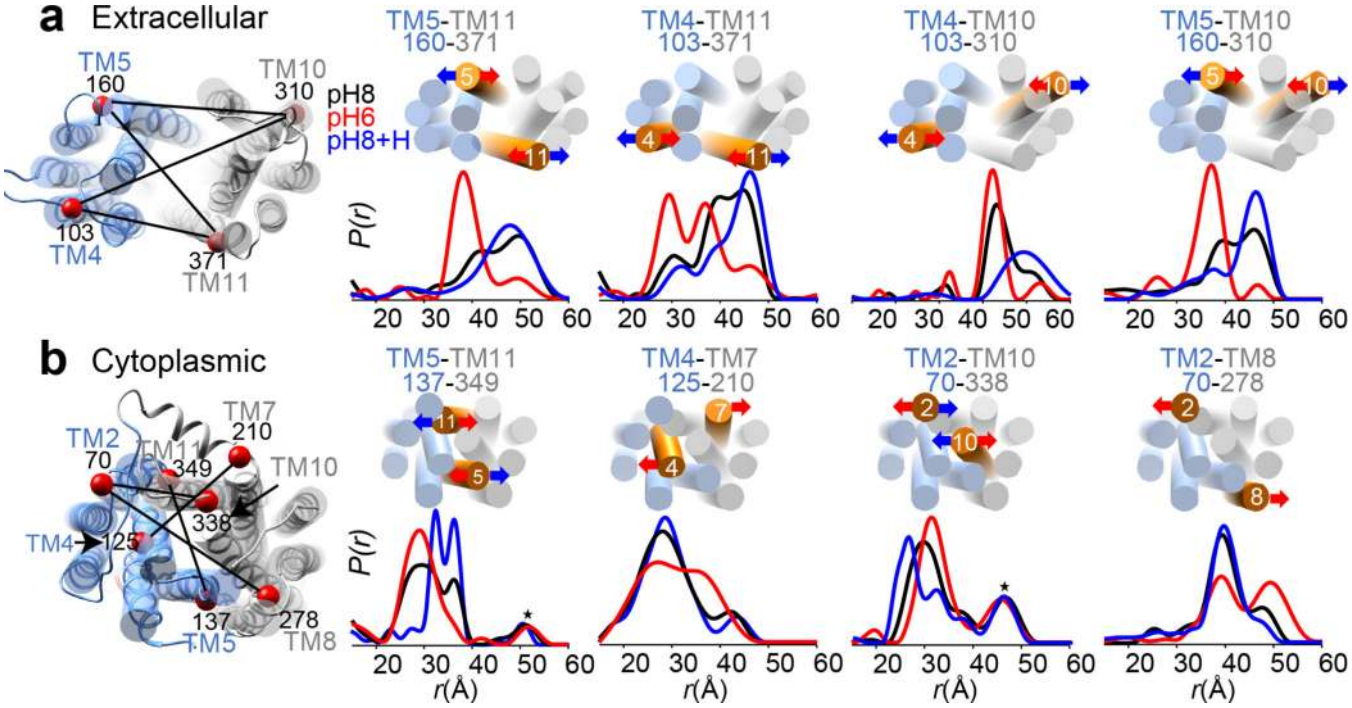

Figure 1. Ligand-dependent conformational changes of LmrP in nanodiscs

(a,b) DEER distance distributions for spin labeled cysteine pairs between the N- and C-lobes located on the extracellular (a) and cytoplasmic (b) ends of TM helices, obtained at pH8 (black), pH6 (red) and pH8 + 1mM Hoechst 33342 (blue). Distributions were normalized: r indicates interspin distance; *P(r)* indicates the distance probability, asterisks denote peaks resulting from partial aggregation observed in some samples upon concentration (see Methods). The closing or opening upon ligand binding is indicated by colored arrows (red: proton binding, blue: Hoechst 33342 binding) with targeted helices in orange. Left: LmrP homology model with cysteine pairs highlighted in red, connected by a line, with TM numbers indicated on top - view from the extracellular (a) or cytoplasmic (b) side. The N-lobe is colored blue and the C-lobe is colored grey. Source data for graphs are available online.

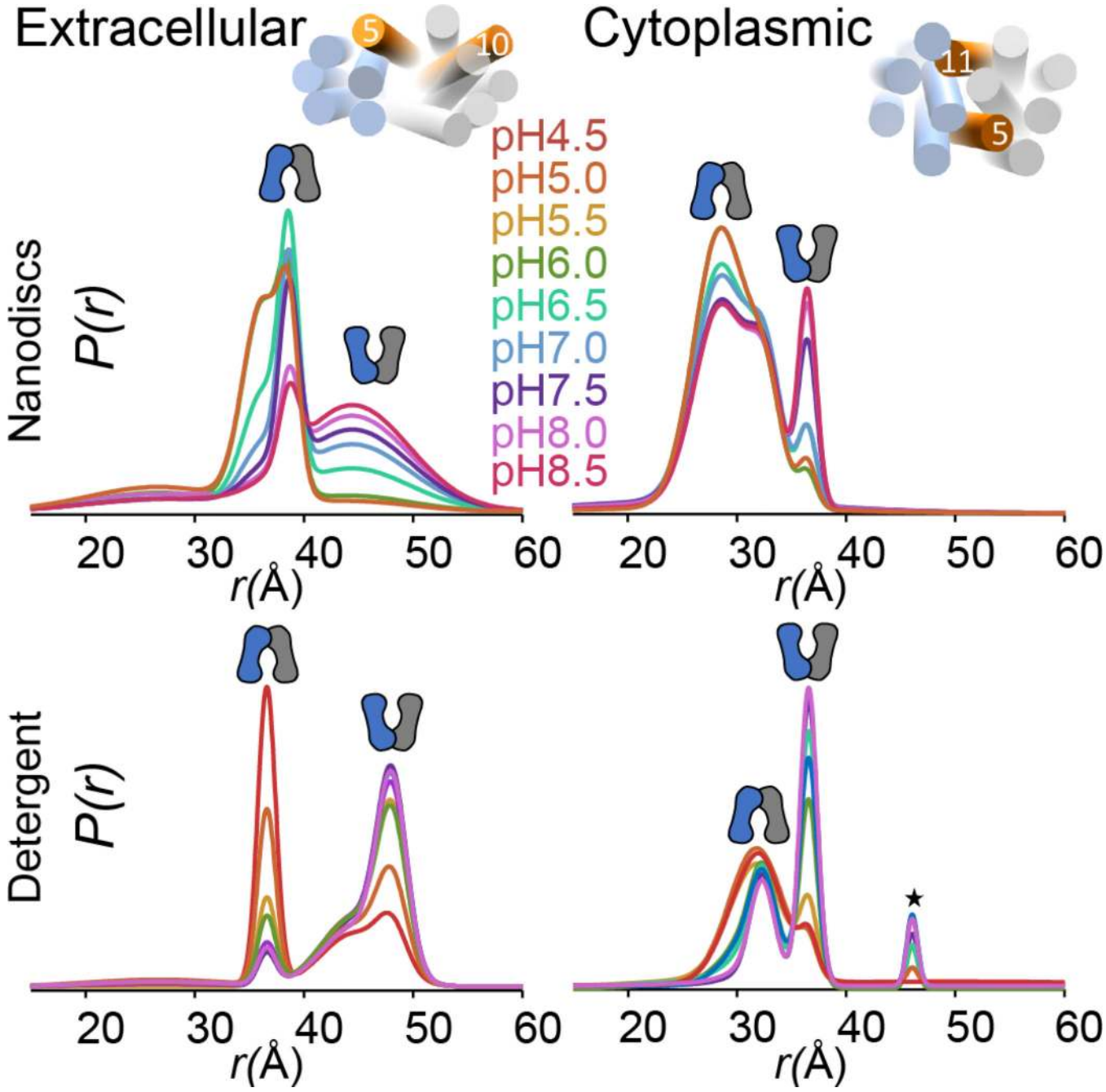

Figure 2. The lipid environment favors the inward-open conformation

DEER distance distributions of the $160R_1$-$310R_1$ and the $137R_1$-$349R_1$ pairs, used as extracellular (left) and cytoplasmic (right) reporters, respectively. Top: mutants reconstituted in *E.coli* polar lipids nanodiscs, at pH values ranging from pH5 to pH8.5 in 0.5 unit increments. Bottom: mutants in detergent micelles, at pH values ranging from pH4.5 to pH8 in 0.5 unit increments. Source data for graphs are available online.

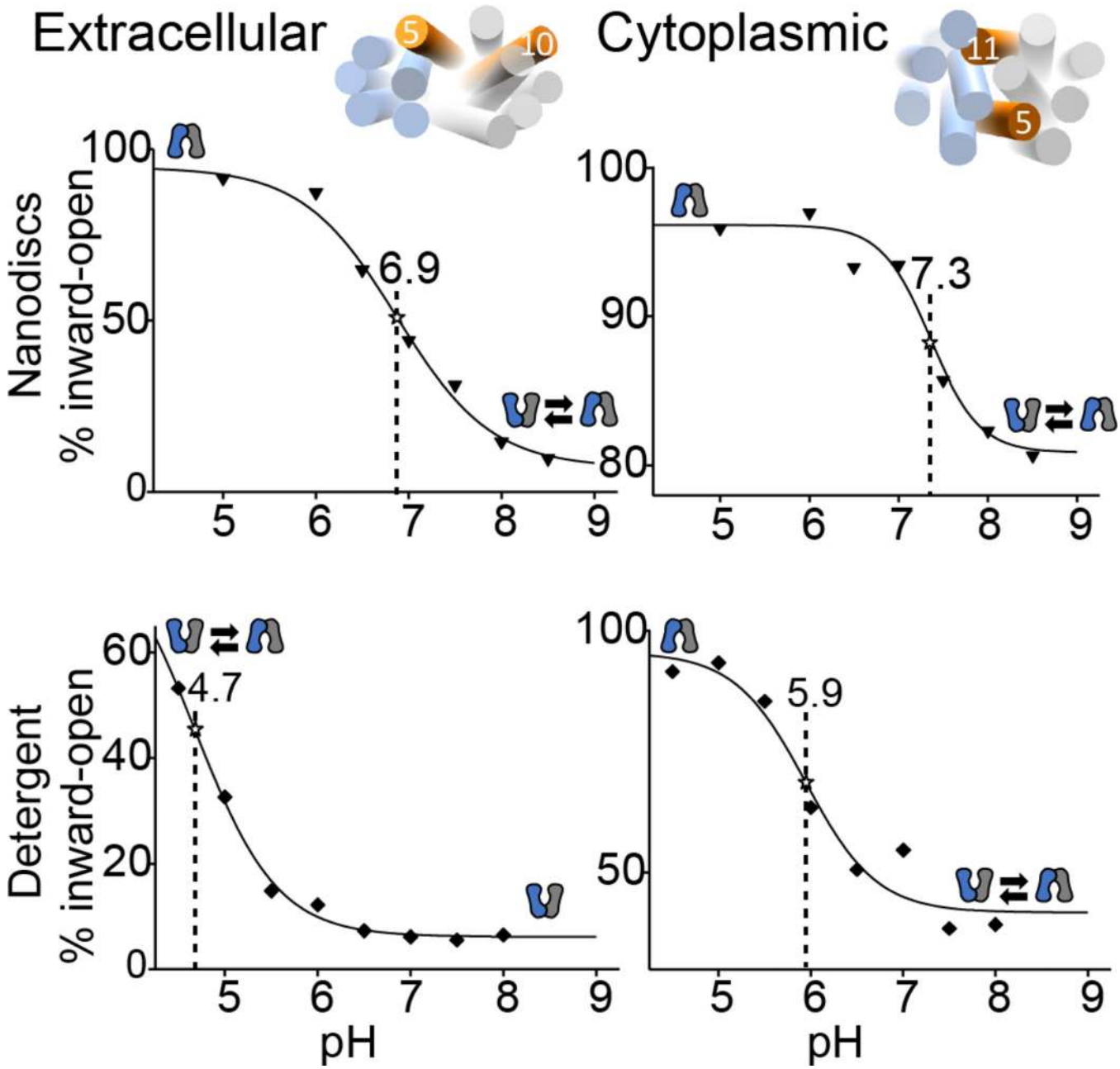

Figure 3. The lipid environment increases the pK of LmrP conformational transition

The fraction of the inward-open component(s) of the distance distributions for the extracellular reporter ($160R_1$-$310R_1$, left) and cytoplasmic reporter ($137R_1$-$349R_1$, right), as determined by global analysis of the raw data, is plotted as a function of pH and fitted with a sigmoidal dose-response curve. The top and bottom panels represent the pH-dependence of the distance distribution in nanodiscs and detergent micelles, respectively. Source data for graphs are available online.

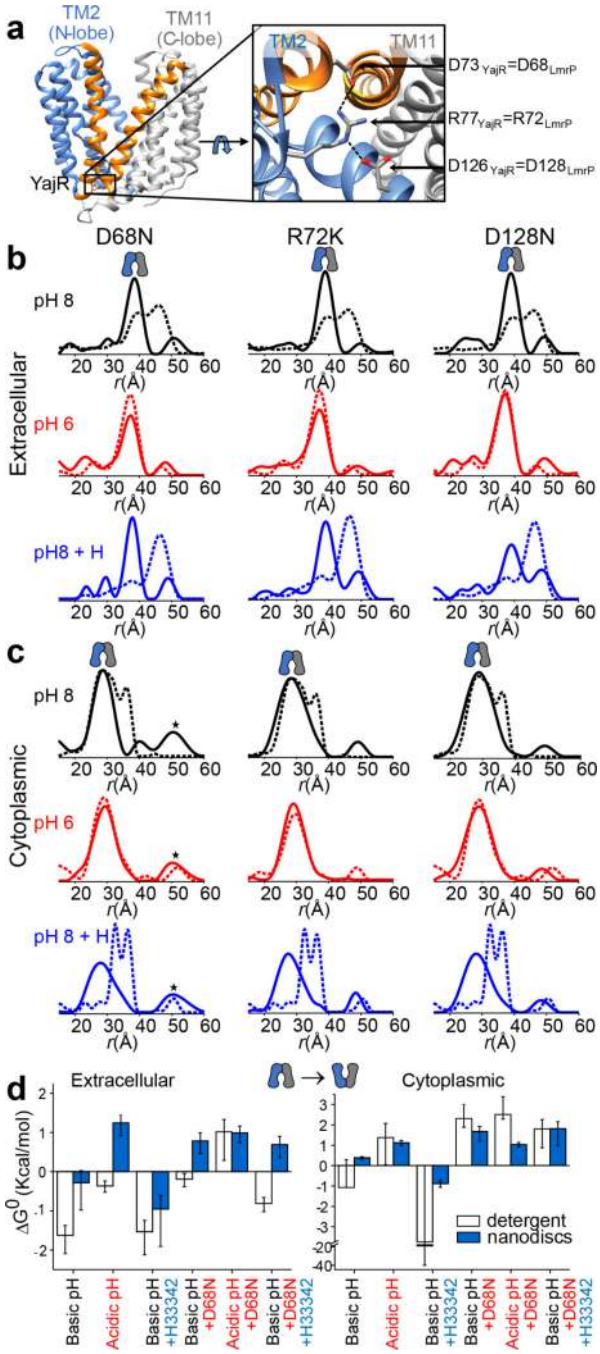

Figure 4. Disruption of the charge-relay network favors the inward-open conformation in nanodiscs

(a) Crystal structure of the LmrP homolog YajR in the outward-open conformation. The charge-relay network of conserved residues is highlighted. TM2 and TM11 are displayed in orange. The cytoplasmic domain of YajR was removed for clarity. (b,c) Single mutations D68N, R72K and D128N combined with extracellular (b) ($160R_1$-$310R_1$) and cytoplasmic (c) ($137R_1$-$349R_1$) reporters. DEER measurements carried out at pH6 (red), pH8 (black), and pH8 + Hoechst 33342 (blue) in the absence (dashed line) and presence (solid line) of each mutation. (d) ΔG° of the conformational transition for the extracellular reporter

(160R1-310R1, left) and cytoplasmic reporter (137R1-349R1, right), as a function of the environment (blue: *E.coli* polar lipids nanodiscs - white: β-DDM detergent). See methods for calculation of ΔG° and associated errors. The error bars are obtained by propagating the fit errors for the amplitude of the individual components of the distance distributions. Source data for graphs are available online.

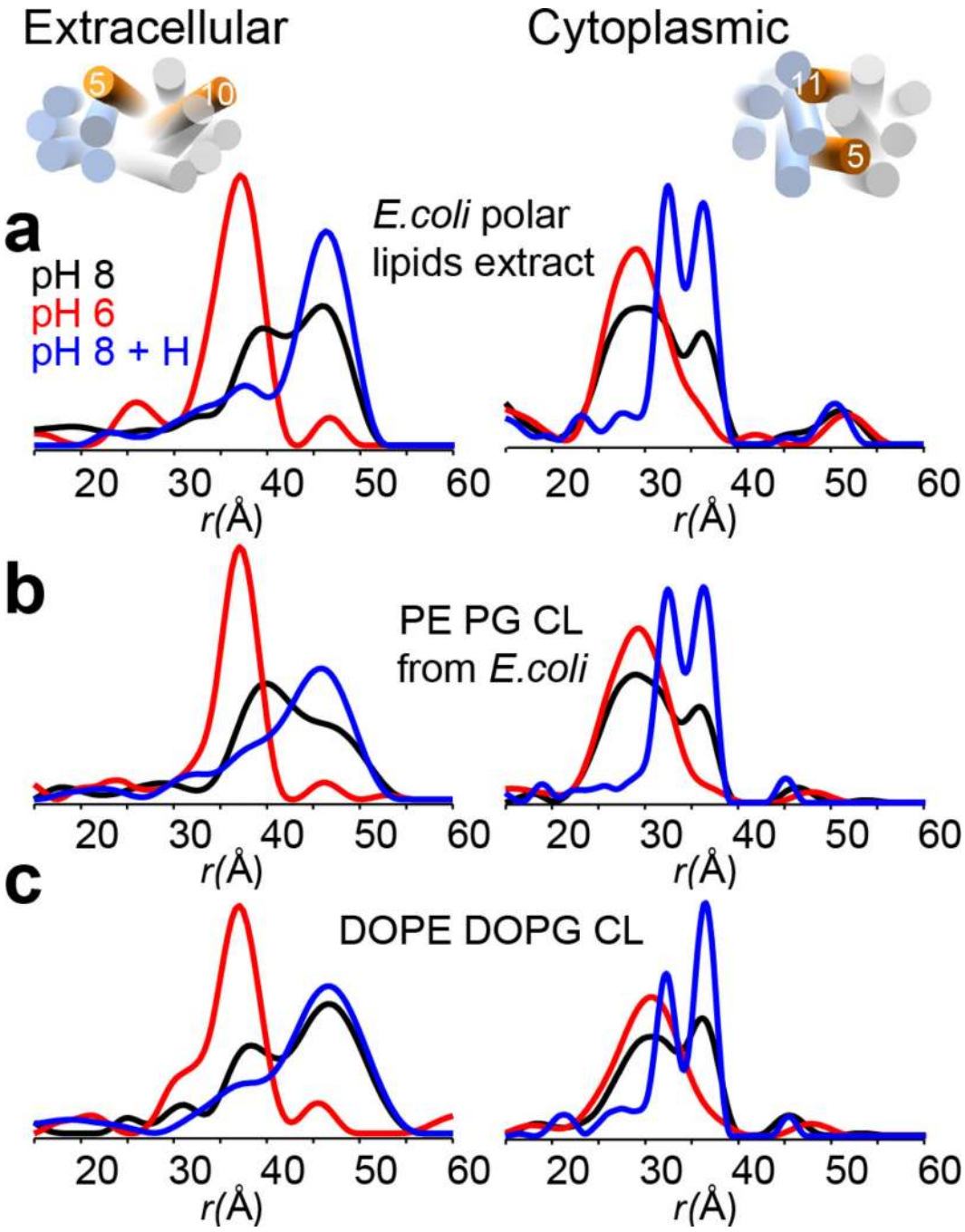

Figure 5. Differences in the fatty acid chain length and structure cause minor changes of the conformational equilibrium

DEER distance distributions of the $160R_1$-$310R_1$ and the $137R_1$-$349R_1$ pairs, used as extracellular (left) and cytoplasmic (right) distance reporters, respectively. Distance distributions at pH8 (black), pH6 (red), pH8 + Hoechst 33342 (blue) in (a) *E.coli* polar lipid extract, (b) combination of PE, PG and CL extracts of *E.coli*, and (c) combination of synthetic DOPE, DOPG and CL. Source data for graphs are available online.

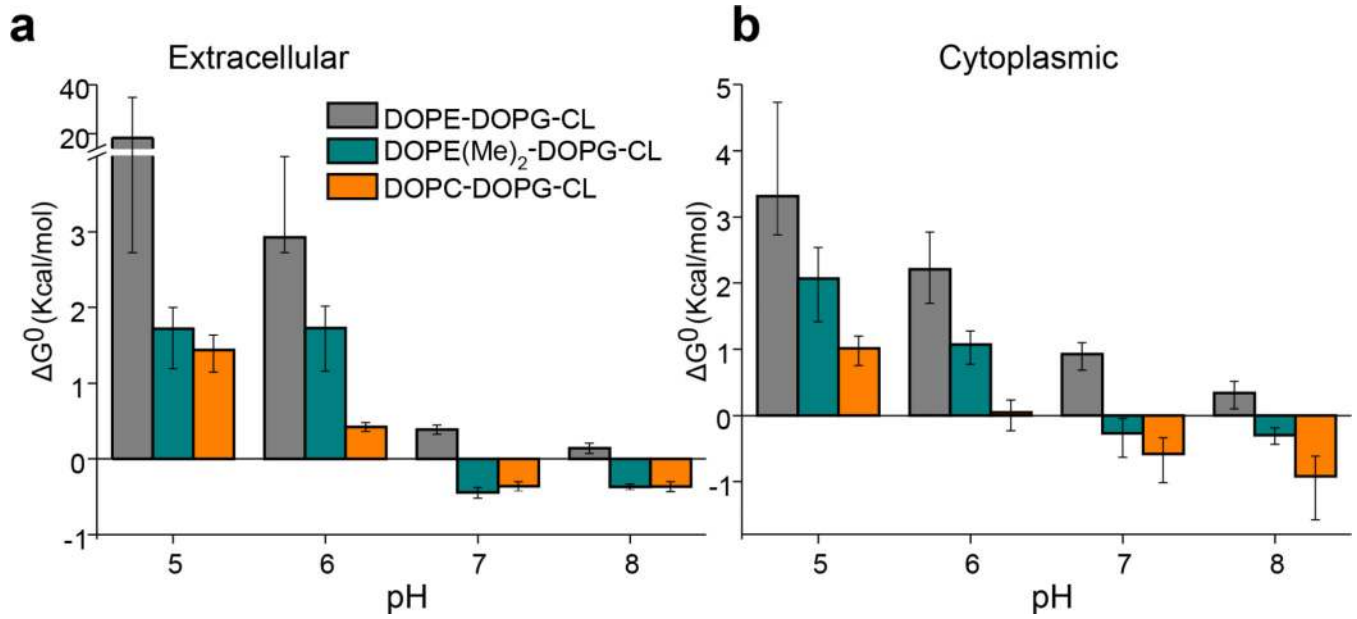

Figure 6. Incremental methylation of phosphatidylethanolamine headgroup stabilizes the outward-open conformation

(a,b) ΔG° of the transition as a function of the pH and the lipid composition. (a) extracellular distance reporter $160R_1$-$310R_1$. (b) cytoplasmic distance reporter $137R_1$-$349R_1$. In order of decreasing ΔG° values: DOPE-DOPG-CL (grey)> $DOPE(Me)_2$-DOPG-CL (blue) > DOPC-DOPG-CL (orange). See methods for calculation of ΔG° and associated errors. The error bars are obtained by propagating the fit errors for the amplitude of the individual components of the distance distributions. Source data for graphs are available online.

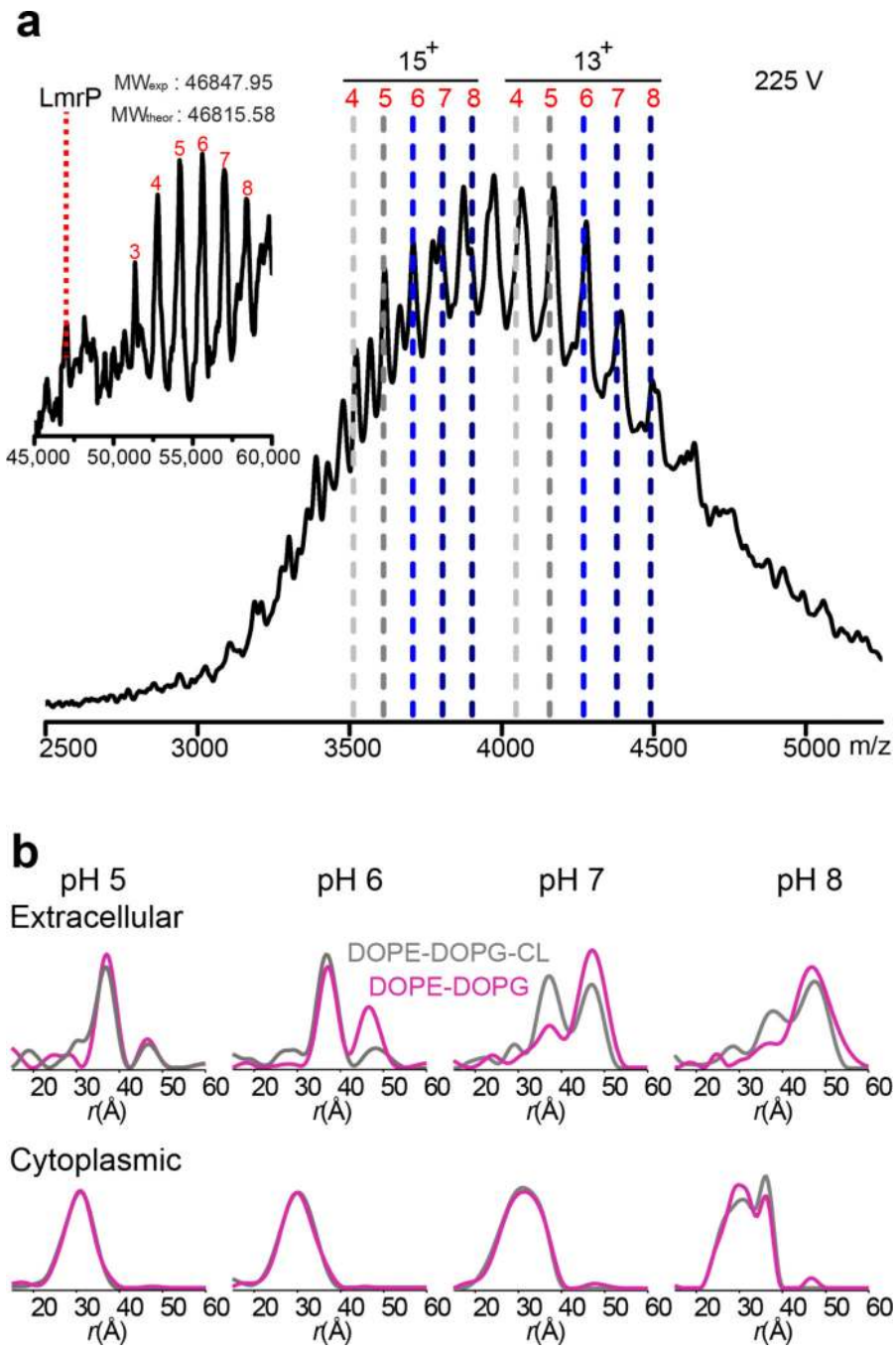

Figure 7. Cardiolipin binds to LmrP with high-affinity and highlights conformational decoupling between the two sides of the transporter

(a) Positive mode nano-ESI MS. Although a charge state distribution from 11^+ to 17^+ is observed, only the 13^+ and 15^+ peaks are indicated for clarity by dotted lines representing the theoretical m/z values, with red numbers corresponding to the number of cardiolipin molecules bound. The inset shows the deconvoluted mass spectrum with up to eight CL bound. The red dotted line indicates the mass of free LmrP. (b) distance distributions of the extracellular $160R_1$-$310R_1$ (top panels) and cytoplasmic $137R_1$-$349R_1$ (bottom panels)

reporters reconstituted in nanodisc with (grey) and without (pink) 10% CL. Source data for graphs are available online.